Published in final edited form as:
*JACC Cardiovasc Interv*. 2011 December ; 4(12): 1326–1334. doi:10.1016/j.jcin.2011.09.012.

# Closed-Chest Transthoracic Magnetic Resonance Imaging-Guided Ventricular Septal Defect Closure in Swine

**Kanishka Ratnayaka, MD**[*,†], **Christina E. Saikus, PhD**[*], **Anthony Z. Faranesh, PhD**[*], **Jamie A. Bell, BSE**[*], **Israel M. Barbash, MD**[*], **Ozgur Kocaturk, PhD**[*], **Christine A. Reyes, MD**[†], **Merdim Sonmez, MS**[*], **William H. Schenke, BS**[*], **Victor J. Wright, BS**[*], **Michael S. Hansen, PhD**[*], **Michael C. Slack, MD**[†], and **Robert J. Lederman, MD**[*]

[*]Cardiovascular and Pulmonary Branch, Division of Intramural Research, National Heart, Lung, and Blood Institute, National Institutes of Health, Bethesda, Maryland [†]Cardiology Division, Children's National Medical Center, Washington, DC

## Abstract

**Objectives—**The aim of this study was to close ventricular septal defects (VSDs) directly through the chest wall using magnetic resonance imaging (MRI) guidance, without cardiopulmonary bypass, sternotomy, or radiation exposure.

**Background—**Surgical, percutaneous, and hybrid management of VSD each have limitations and known morbidity.

**Methods—**Percutaneous muscular VSDs were created in 10 naive Yorkshire swine using a transjugular laser catheter. Under real-time MRI guidance, a direct transthoracic vascular access sheath was introduced through the chest into the heart along a trajectory suitable for VSD access and closure. Through this transthoracic sheath, muscular VSDs were occluded using a commercial nitinol device. Finally, the right ventricular free wall was closed using a commercial collagen plug intended for arterial closure.

**Results—**Anterior, posterior, and mid-muscular VSDs (6.8 ± 1.8 mm) were created. VSDs were closed successfully in all animals. The transthoracic access sheath was displaced in 2, both fatal. Thereafter, we tested an intracameral retention sheath to prevent this complication. Right ventricular access ports were closed successfully in all, and after as many as 30 days, healed successfully.

**Conclusions—**Real-time MRI guidance allowed closed-chest transthoracic perventricular muscular VSD closure in a clinically meaningful animal model. Once applied to patients, this approach may avoid traditional surgical, percutaneous, or open-chest transcatheter ("hybrid") risks.

### Keywords

hybrid surgical procedures; imaging in the catheterization laboratory; interventional cardiology; interventional MRI; perventricular; ventriculoseptal defect



**Reprint requests and correspondence:** Dr. Robert J. Lederman, Cardiovascular and Pulmonary Branch, Division of Intramural Research, National Heart, Lung, and Blood Institute, National Institutes of Health, Building 10, Room 2c713, MSC1538, Bethesda, Maryland 20892-1538. lederman@nih.gov. .

APPENDIX For accompanying videos, please see the online version of this article.

All other authors have reported that they have no relationships relevant to the contents of this paper to disclose.

Ventricular septal defects (VSDs) represent the most common congenital heart abnormalities managed in childhood and are also common in adults (1). Traditional surgical VSD repair requires sternotomy, cardiopulmonary bypass, and blood products. Right ventricular trabeculation or apical position can make these defects difficult to locate and close completely. After surgical repair, one-quarter have persistent, residual lesions (2). In some settings (i.e., post-infarction, iatrogenic, or post-traumatic VSDs), surgery may be unattractive.

Percutaneous catheter-based VSD closure, an alternative to surgery, suffers from radiation exposure and limited visualization, even with adjunctive echocardiography. Furthermore, children may have prohibitively small access vessels or may suffer hemodynamic compromise (3) during transcatheter attempts. Hybrid (open-chest transcatheter) procedures aim to address these limitations, at the expense of surgical morbidity.

Real-time magnetic resonance imaging (MRI) guidance might overcome the deficiencies of surgical, percutaneous, and hybrid approaches by affording surgical type exposure without surgical risk (4). We hypothesized that muscular VSDs could be repaired with little morbidity using closed-chest transthoracic MRI-guided techniques.

## Methods

### Animal Procedures

Animal procedures were approved by the National Heart, Lung, and Blood institutional animal care and use committee. Nineteen naive Yorkshire swine (Archer Farms, Darlington, Maryland; 46.5 ± 10.1 kg) were anesthetized and mechanically ventilated. Percutaneous arterial, venous, and subxiphoid pericardial access was obtained. Experiments were conducted in a combined interventional cardiovascular MRI and x-ray fluoroscopy suite (1.5-T Espree, Axiom Artis; Siemens, Erlangen, Germany) (4). Heparin maintained activated clotting times >250 s.

### Percutaneous Animal Model of Muscular VSD Using an Excimer Laser Sheath

Muscular VSD was created using coregistered x-ray and MRI roadmaps (5) (x-ray fused with MRI [XFM]) (Figs. 1A to 1C). The target was punctured using a standard 18-ga transseptal needle (Brockenbrough, Medtronic, Minneapolis, Minnesota) (Figs. 1A and 1B). An 0.018-in guidewire (V-18, Boston Scientific, Natick, Massachusetts) was delivered to the left ventricle. It was snared using a catheter passed retrograde across the aortic valve. The wire was exteriorized through the femoral arterial sheath creating an “arterio-venous loop.” A 16-F excimer laser catheter intended to extract pacemaker leads (SLS-II, Spectranetics, Colorado Springs, Colorado) was activated in multiple passes over the guidewire to create a muscular VSD (Fig. 1C). The defect size was measured using radiocontrast angiography and by MRI (Fig. 1D). The degree of left to right shunt was measured by Fick oximetry and by velocity-encoded MRI.

### Magnetic Resonance Imaging

Steady-state free precession (SSFP) imaging followed usual parameters: repetition time (TR)/echo time (TE), 3.2/1.5 ms; flip angle, 80°; bandwidth, 930 Hz/pixel; field of view (FOV), 340 × 276 mm; matrix, 192 × 156 pixels; slice thickness, 6 mm. Typical “black-blood” turbo spin echo images used TR/TE, 700/34 ms; flip angle, 180°; bandwidth, 292 Hz/pixel; FOV, 340 × 276 mm; matrix, 256 × 125 pixels; slice thickness, 6 mm. Typical velocity-encoded gradient echo acquisition parameters were TR/TE, 12.8/2.9 ms; flip angle,

30°; bandwidth, 434 Hz/pixel; FOV, 370 × 220 mm; matrix, 256 × 88 pixels; slice thickness, 6 mm, Nyquist limit, 100 to 125 cm/s.

VSD dimensions were measured during systole on representative short-axis or long-axis SSFP images, and the largest dimension was chosen for device sizing.

Real-time MRI for interventional procedures used SSFP with TR/TE, 2.8/1.4 ms; flip angle, 60°; bandwidth, 800 Hz/pixel; matrix, 192 × 108; and FOV, 32 × 24 cm.

## "Active" MRI Catheter Devices

Interventional devices were visualized as "active" antennae incorporating MRI receiver coils. We have found these more conspicuous than "passive" devices that are visualized based on intrinsic materials properties (4).

To provide clear delineation of the needle tip and shaft location during access, we used an actively visualized needle. An MRI needle incorporated an elongated loop coil and multiple tight windings to enhance visibility (Figs. 2 and 3) (6).

"Passive" hydrophilic coated nitinol guidewires (Terumo, Somerset, New Jersey) were used for wire exchange. VSD were crossed with a loop-less-design, "active" 0.035-in guidewire (Fig. 3) (7).

The marketed occluder device (Amplatzer Muscular VSD Occluder, AGA Medical, Plymouth, Minnesota) incorporates a stainless-steel microscrew hub to mate with a delivery cable. To avoid large MRI artifacts, the steel microscrew hub was replaced (courtesy of AGA Medical) with a custom titanium microscrew on 8-mm occluders.

We developed an active MRI delivery cable to enhance visibility of the modified VSD occluder during real-time MRI (Fig. 3). A mating titanium microscrew was laser welded to the active MRI delivery cable tip (7). The loop-less-design cable was tuned and matched with the implant to change cable signal during sequential disk expansion and upon release.

## MRI-Guided Procedure

**Closed-chest transthoracic MRI-guided cardiac access—**Real-time SSFP MRI guided all procedural steps. Two orthogonal (short- and long-axis) slices were selected to represent the VSD to the operator along a desired trajectory, with simultaneous volume-rendering of the slices in their 3-dimensional position (Fig. 2).

A large field of view allowed extrathoracic maneuvers to be viewed interactively. First, a trajectory was planned by selecting a skin entry site and a predicted right ventricular entry site intended to facilitate later crossing of the ventricular septal defect. Next, the active needle was introduced through the skin and chest wall into the right ventricle (RV) and exchanged over a passive nitinol guidewire for a passive 9-F introducer sheath. Sheath position was confirmed using 5 ml (1%) gadopentetate-dimeglumine injection (Magnevist, Bayer, Wayne, New Jersey) during real-time saturation-prepared MRI.

**Transthoracic MRI-guided muscular VSD closure—**With a transthoracic right ventricular introducer sheath in place, the operator manipulated the active guidewire across the muscular VSD into the left ventricle. Over this wire, the introducer sheath was delivered into the left ventricle and its position confirmed with a hand injection of dilute gadopentetate. The modified 8-mm AGA muscular VSD occluder device—mounted on the active delivery cable—was then delivered to the muscular VSD in standard fashion (3) (Fig. 3).

**Transthoracic MRI-guided RV free wall closure—**An off-the-shelf 8-F absorbable collagen vascular closure device (Angio-Seal VIP, St. Jude Medical, Minnetonka, Minnesota) was used to close the RV free wall under real-time MRI (Fig. 4) (8). We created "permissive pericardial tamponade" by instilling saline through the pre-positioned pericardial drain to separate the visceral and parietal pericardium and assure delivery of the external collagen to the epicardial surface. Afterwards, the pericardial fluid was evacuated.

### Experimental Design and Data Analysis

Once the animal model was developed, we attempted to close the VSD in 2 nonsurvival animals and then in 8 animals to survive 2 days or 1 month. We performed interval imaging and catheterization followed by necropsy and histopathology.

Blood was tested using bedside human assays for chemistry (i-Stat, Abbott, Princeton, New Jersey), oximetry (Avox, San Antonio, Texas), and coagulation (Hemachron, ITC, Edison, New Jersey).

Effusions were measured by maximal dimension in multiplanar MRI. *RV sheath placement time* began when the active needle was placed on the chest wall until placement was confirmed with selective gadopentetate injection. *VSD crossing time* was from the active wire insertion until LV sheath placement was confirmed with selective gadopentetate injection. *Occluder deployment time* started with the introduction of the delivery system and ended with device release. *RV free wall closure* started with positioning the vascular sheath in RV and ended with aspiration of pericardial fluid after vascular closure device deployment. Total procedural time was defined by the start of *RV sheath placement time* and conclusion of *RV free wall closure*.

Results are expressed as mean ± SD.

## Results

### Animal model

We attempted to create a muscular VSD in 19 animals, and failed in 2 because of cardiac perforation or refractory ventricular fibrillation. In the first 2 animals with successful muscular VSD creation, closure was not attempted. In 5 animals, the resulting VSD was too large, and animals suffered acute heart failure before the lesion could be treated.

We attempted VSD closure in the 10 remaining animals in 3 phases: nonsurvival initial feasibility (n = 2), survival for 2 days (n = 4), and survival for 30 days (n = 4). The maximum VSD dimension was 6.8 ± 1.8 mm by radiocontrast angiography and 5.1 ± 0.8 by SSFP MRI. The defects were located in the following septal locations: anterior (n = 2), posterior (n = 5), and midmuscular (n = 3). Intracardiac shunts (pulmonary vs. systemic blood flow or Qp/Qs) were mild (1.1 ± 0.3 by Fick technique, 1.2 ± 0.2 by velocity-encoded MRI). Creating the defect model also led to small acute pleural and pericardial effusions (Table 1).

### Transthoracic cardiac access

Real-time MRI successfully guided active needle access, wire exchange, and delivery of 9-F introducer sheaths into the RV in all animals. Multiple interactive imaging planes allowed selection of an optimal needle trajectory (Fig. 2, Online Video 1). RV sheath placement required 8.5 ± 5.3 min. This was not associated with sustained arrhythmia or hemodynamic change.

### Transthoracic MRI-guided muscular VSD closure

Muscular VSD device closure was achieved in all animals (n = 10) (Fig. 3, Online Video 2). Real-time MRI guided post-deployment positioning to avoid critical structures, such as atrioventricular valves. Procedural times for each step were VSD crossing time (10.2 ± 13.7 min), occluder deployment time (7.8 ± 5.7 min). Activated clotting times were 407 ± 205 s. Animals were hemodynamically stable, with no sustained arrhythmias documented.

In 1 animal, real-time MRI demonstrated inadvertent entrapment of a mitral subvalvar element (Online Video 3), and guided repositioning.

### Transthoracic MRI-guided RV free wall closure

Right ventricular free wall closure, when attempted, was successful in all animals (n = 6; 6.2 ± 6.5 min). Permissive pericardial tamponade entailed temporary instillation of normal saline (150 ± 42.4 ml) to facilitate appropriate delivery and deployment of the collagen sponge, followed by withdrawal of serosanguinous fluid (155 ± 35.4 ml) (Fig. 4, Online Video 4).

The total procedure time, from initial needle access to final RV closure, was 77.2 ± 27.4 min.

### Complications and mitigation approach

Two animals died despite successful VSD closure as complications of “lost” access to the right ventricular cavity before an attempt at nonsurgical access port closure, 1 each intended for 2- and for 30-day survival, respectively.

We observed that inadvertent sheath withdrawal from the small right ventricular cavity was related to sheath retraction to expose and deploy the right ventricular disk of the closure device, exacerbated by respiratory and cardiac motion.

We sought a device to secure the sheath into the RV, especially during deployment of the right ventricular disk. We found a commercial balloon-tipped right ventricular intracameral retention sheath (IABC, Cook Medical, Bloomington, Indiana) to be suitable to prove the concept (Fig. 5). This afforded reliable right ventricular intracameral access, as well as effective pericardial layer separation during permissive pericardial tamponade.

### Procedural and post-intervention surveillance

In follow-up, no animal showed evidence of coronary artery injury manifest as electrocardiographic injury current or wall motion abnormality. No coronary ischemia occurred. One animal experienced transient heart block after device implantation that self-resolved. No significant atrioventricular valve regurgitation was detected early or in follow-up.

Follow-up data are presented in Table 1. No significant residual muscular VSD shunt was detected after occluder release. Follow-up imaging showed good occluder position (Fig. 6). Two animals in the 1-month survival group had small pericardial effusions (hemodynamically insignificant) drained after surveillance MRI (2 days post-intervention). Pericardial effusions did not recur.

### Necropsy and histopathology

Gross pathology revealed appropriate placement and endothelization of the VSD occluder device (Fig. 7). No atrioventricular or semilunar valve apparatus was entrapped by the device. In swine surviving for 2 days, components of the vascular closure device were

visible and found in the expected position. One animal had the collagen plug deployed outside the pericardium. In animals surviving for 1 month, the collagen plug had resorbed and was no longer identifiable on epicardial surface. Partial remnants of the copolymer anchor were visualized on the endocardial surface.

Histopathology survey (hematoxylin and eosin stain) compared the right ventricular free wall at the closure site and distal to closure site. The epicardial surface was similarly mildly fibrotic at both sites. In contrast to the distal site, inflammatory changes at the closure site were noted in a predominately subendocardial location. Fibrosis (highlighted by trichrome stain), edema, lymphocytic infiltrate, and foreign body giant cell reaction were limited to this immediate location (Fig. 7).

## Discussion

We showed direct transthoracic VSD repair to be feasible under real-time MRI guidance. MRI depicted the defect, the heart surface, and the chest wall in relation to each other for planning and execution of needle, guidewire, and catheter traversals into both right and left ventricular cavities. Real-time MRI also provided straightforward visualization of all steps of closure: device delivery, deployment, and release. Equally important, real-time MRI depicted structures in context in a way we find qualitatively superior to x-ray and ultrasound guidance of conventional nonsurgical structural heart procedures, because the heart, thorax, pleura, and pericardium are displayed instantaneously throughout.

Our closed-chest real-time MRI-guided transthoracic VSD repair approach offers an alternative for small children in whom percutaneous options are not possible (vascular access) or pose unnecessary risk of major adverse outcomes (arrhythmia, hemodynamic compromise, cardiac perforation, tamponade, death) (3). It may avert cardiopulmonary bypass required in traditional VSD surgical repair or sternotomy required even in hybrid perventricular approaches.

In this preclinical experience with single “intentional” defects, all VSD closure procedures were successful. We did not encounter known complications of traditional (percutaneous, hybrid) VSD device closure, such as device embolization, residual shunt, atrioventricular valve distortion, ventricular dysfunction, or left ventricular free wall damage (2,9–11). Nor did we observe damage to coronary, pleural, or intercostal arteries during percutaneous access (12).

Even in this preliminary experience, procedure planning and conduct was completed in a little more than 1 h. This compares favorably with hybrid surgical (11,13) and percutaneous (2,10) approaches.

The marketed AGA medical VSD occluder and its matching delivery cable each have a small stainless steel microscrew hub that distorts MR images. In collaboration with the manufacturer, the microscrews were replaced with titanium to eliminate the steel susceptibility artifact.

We further customized the delivery cable as an active antenna device tuned to couple with the nitinol occluder in the partially and fully deployed positions. This novel approach to deliberate coupling significantly enhanced visibility and performance of the device.

We were able to close 9-F access port holes in the RV using a commercial vascular closure device, as has been described in case reports (14). Our “permissive pericardial tamponade” technique facilitated appropriate deployment of the collagen sponge on the epicardial surface (8), but failed without sequelae in 1 case. Two animals had small pericardial

effusions, which we drained on day 2 and which did not recur. Similar pericardial collections are noted after "hybrid" VSD closure (11). Gross pathology and histology at 1 month showed excellent healing of the access site and resorption of the copolymer anchor. By contrast, we have found this same collagen-based closure device to be unsuitable for closure of left ventricular access ports, and many operators report serious consequences of simple sheath withdrawal without surgical or device closure after transapical puncture for interventional procedures (15). Custom epicardial closure solutions are under development using sutures, staples, and other approaches.

The chief procedural limitation in our experience was inadvertent loss of right ventricular access after VSD device delivery, which proved lethal in 2 animals. We found an alternative sheath solution that promises to mitigate this limitation, by providing a secure "lock" of the sheath tip inside the right ventricle when necessary. In addition, it can help to separate visceral and parietal pericardium during access port closure. Lower-profile intracameral retention sheaths are feasible.

The early nonrecurrent pericardial bleeding we experienced might be less important in clinical practice, where mitigation options include blood transfusion, reversal of anticoagulation (intentionally avoided in these experiments to "stress" hemostasis), temporary post-procedure pericardial drain catheters, and surgical repair if indicated.

We created a new animal model of VSD using percutaneous catheter techniques and MRI–x-ray co-registration. We had been unsuccessful using echocardiographic guidance because of poor acoustic windows. Before debulking myocardium using the excimer laser sheath extraction catheter, we had been unsuccessful in creating a sustained ventricular communication even using large conventional (up to 18 mm) or cutting (up to 6 mm) angioplasty balloons. Nevertheless, these naive animals suffered acute hemodynamic instability, accounting for significant procedural mortality during model creation. The acute physiology in this model resembled post-infarction, traumatic, and iatrogenic lesions. Our animal model challenged us to target, cross, and close small defects compared with technically easier larger chronic defects, in the range reported for hybrid (11) and percutaneous (2,10) closure. That said, we were not able to create apical VSD.

We showed that a real-time MRI-guided direct transthoracic procedure is feasible. Clinical translation would require further development of the titanium microscrews, assurance of no heating during MRI, and adjunctive catheter tools, such as an enhanced-conspicuity delivery sheath and "buddy" guidewires to enhance procedure safety.

Our transthoracic approach may be suitable for membranous (16) and less common subarterial VSDs (13). Related applications for complex congenital interventions include transventricular atretic pulmonary valve perforation and transatrial septal perforation/septostomy. With suitable devices, real-time MRI could facilitate percutaneous VSD repair in larger children.

## Conclusions

Real-time MRI guided successful closed-chest transthoracic muscular VSD closure in a swine model. This approach may avoid traditional surgical, percutaneous, or open-chest transcatheter ("hybrid") risks. In the future, it may facilitate or enhance a range of transatrial, transventricular, and intrapericardial structural and electrophysiology cardiac interventions.

## Supplementary Material

Refer to Web version on PubMed Central for supplementary material.

## Acknowledgments

The authors thank Patrick Cooke, Pat Russo, John Oslund, and Kurt Amplatz of AGA Medical Corp. for providing Amplatzer muscular ventricular septal defect (VSD) occluder devices; Katherine Lucas, Joni Taylor for technical assistance.

This work was supported by the Division of Intramural Research (Z01-HL005062-08, Z01-HL006039-01, Z01-HL006041-01), National Heart, Lung, and Blood Institute, National Institutes of Health (NIH). NIH and Siemens Medical Systems have a collaborative research and development agreement for interventional cardiovascular MRI. AGA Medical supplied devices for closure of ventricular septal defects. Dr. Ratnayaka serves without compensation on a Siemens Pediatric Advisory Council. Dr. Slack receives compensation as a physician training proctor for Amplatzer Medical Corporation.

## Abbreviations and Acronyms

| | |
|---|---|
| **FOV** | field of view |
| **MRI** | magnetic resonance imaging |
| **RV** | right ventricle |
| **SSFP** | steady-state free precession |
| **TE** | echo time |
| **TR** | repetition time |
| **VSD** | ventricular septal defect |
| **XFM** | x-ray fused with magnetic resonance imaging |

## REFERENCES

1. Minette MS, Sahn DJ. Ventricular septal defects. Circulation. 2006; 114:2190–7. [PubMed: 17101870]
2. Dua JS, Carminati M, Lucente M, et al. Transcatheter closure of postsurgical residual ventricular septal defects: early and mid-term results. Catheter Cardiovasc Interv. 2010; 75:246–55. [PubMed: 19908328]
3. Pedra CA, Pedra SR, Chaccur P, et al. Perventricular device closure of congenital muscular ventricular septal defects. Expert Rev Cardiovasc Ther. 2010; 8:663–74. [PubMed: 20450300]
4. Ratnayaka K, Faranesh AZ, Guttman MA, Kocaturk O, Saikus CE, Lederman RJ. Interventional cardiovascular magnetic resonance: still tantalizing. J Cardiovasc Magn Reson. 2008; 10:62. [PubMed: 19114017]
5. Gutiérrez LF, Silva R, Ozturk C, et al. Technology preview: X-ray fused with magnetic resonance during invasive cardiovascular procedures. Catheter Cardiovasc Interv. 2007; 70:773–82. [PubMed: 18022851]
6. Saikus CE, Ratnayaka K, Barbash IM, et al. MRI-guided vascular access with an active visualization needle. J Magn Reson Imaging. 2011; 34:1159–66. [PubMed: 22006552]
7. Ocali O, Atalar E. Intravascular magnetic resonance imaging using a loopless catheter antenna. Magn Reson Med. 1997; 37:112–8. [PubMed: 8978639]
8. Barbash IM, Saikus CE, Ratnayaka K, et al. Limitations of closing percutaneous transthoracic ventricular access ports using a commercial collagen vascular closure device. Catheter Cardiovasc Interv. 2011; 77:1079–85. [PubMed: 21234923]

9. Holzer R, Balzer D, Amin Z, et al. Transcatheter closure of postinfarction ventricular septal defects using the new Amplatzer muscular VSD occluder: results of a U.S. registry. Catheter Cardiovasc Interv. 2004; 61:196–201. [PubMed: 14755811]
10. Al-Kashkari W, Balan P, Kavinsky CJ, Cao QL, Hijazi ZM. Percutaneous device closure of congenital and iatrogenic ventricular septal defects in adult patients. Catheter Cardiovasc Interv. 2011; 77:260–7. [PubMed: 20853354]
11. Michel-Behnke I, Ewert P, Koch A, et al. Device closure of ventricular septal defects by hybrid procedures: A multicenter retrospective study. Catheter Cardiovasc Interv. 2011; 77:242–51. [PubMed: 20517999]
12. Lim DS, Ragosta M, Dent JM. Percutaneous transthoracic ventricular puncture for diagnostic and interventional catheterization. Catheter Cardiovasc Interv. 2008; 71:915–8. [PubMed: 18383174]
13. Chen Q, Chen LW, Wang QM, Cao H, Zhang GC, Chen DZ. Intraoperative device closure of doubly committed subarterial ventricular septal defects: initial experience. Ann Thorac Surg. 2010; 90:869–73. [PubMed: 20732510]
14. Petrov I, Dimitrov C. Closing of a right ventricle perforation with a vascular closure device. Catheter Cardiovasc Interv. 2009; 74:247–50. [PubMed: 19360872]
15. Pitta SR, Cabalka AK, Rihal CS. Complications associated with left ventricular puncture. Catheter Cardiovasc Interv. 2010; 76:993–7. [PubMed: 20928838]
16. Tao K, Lin K, Shi Y, et al. Perventricular device closure of perimembranous ventricular septal defects in 61 young children: early and midterm follow-up results. J Thorac Cardiovasc Surg. 2010; 140:864–70. [PubMed: 20561638]

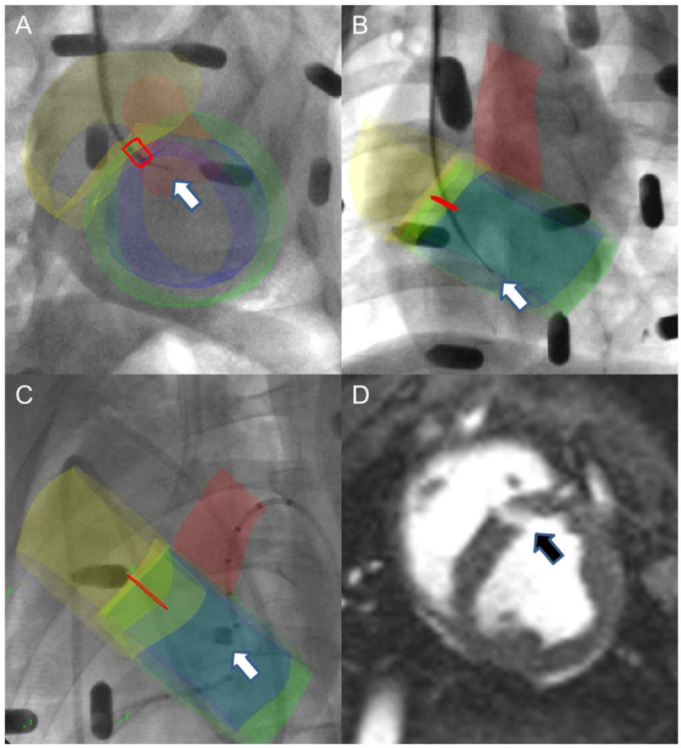


**Figure 1. Percutaneous Muscular VSDs Created Under XFM Guidance**

**(A and B)** X-ray fused with magnetic resonance imaging (XFM) image shows intraprocedure needle **(white arrow)** and target **(red outline)** in 2 orthogonal views. XFM road map includes right **(yellow)** and left **(blue)** ventricular endocardial contours, left ventricular epicardial contour **(green)**, and aortic root **(red)**. **(C)** XFM image shows laser sheath extraction catheter **(white arrow)** during muscular ventricular septal defect (VSD) creation. **(D)** Steady-state free precession (SSFP) “bright blood” image depicts muscular VSD **(black arrow)**.

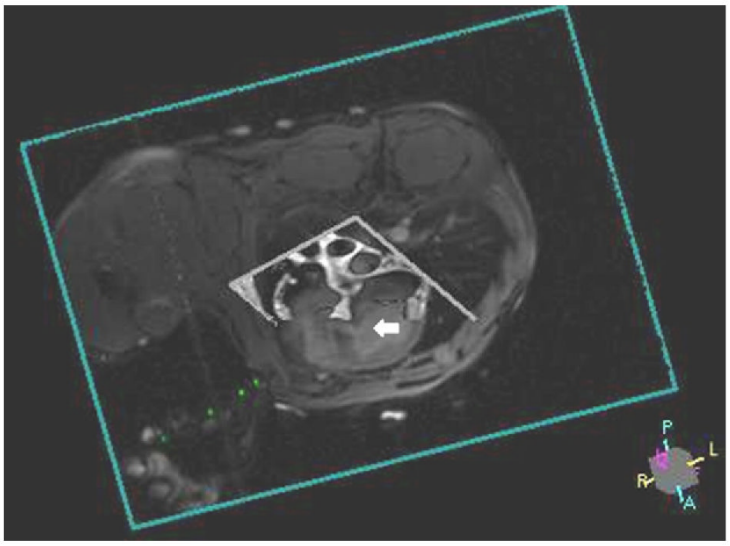


**Figure 2. Real-time MRI Imaging Display During Closed-Chest Transthoracic Needle Access Targeting Muscular VSD**

Three-dimensional rendering of real-time SSFP imaging slice (short axis) and “black-blood” road map (long axis) displays active needle **(green)** targeting mid-muscular VSD **(white arrow)** (Online Video 1). Abbreviations as in Figure 1.

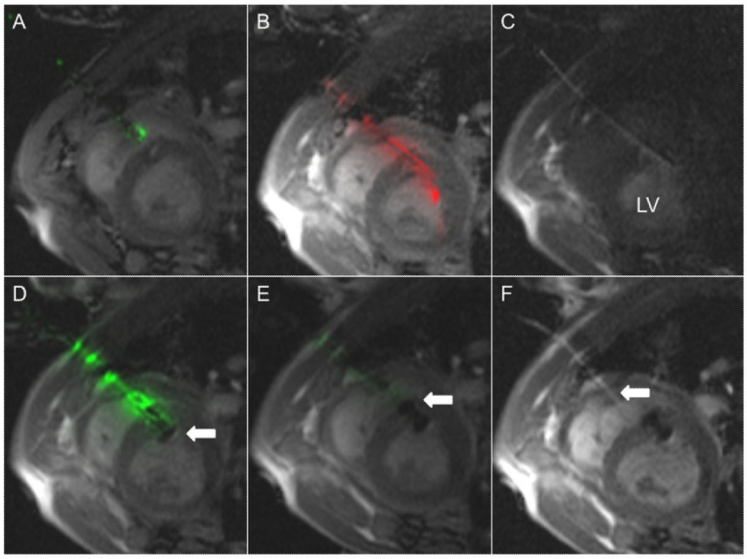


**Figure 3. Real-Time MRI Guidance of Muscular VSD Occluder Delivery**

**(A)** "Active" needle **(green)** puncture through the chest wall and the right ventricular free wall into the right ventricular cavity, avoiding septal injury/puncture. **(B)** "Active" guidewire **(red signal)** is used for crossing VSD. **(C)** Dilute gadolinium injection confirms left ventricle (LV) sheath placement. **(D)** Modified VSD occluder device is mounted on "active" delivery cable **(green)** and delivered to the defect. First, the left ventricular disk **(white arrow)** is deployed. **(E)** Next, the right ventricular disk **(white arrow)** is deployed. "Active" delivery cable **(green)** is tuned such that signal attenuation occurs with full device delivery. **(F)** Finally, the device is released (Online Videos 2 and 3). Dilute gadolinium highlights the access sheath **(white arrow)**. Abbreviations as in Figure 1.

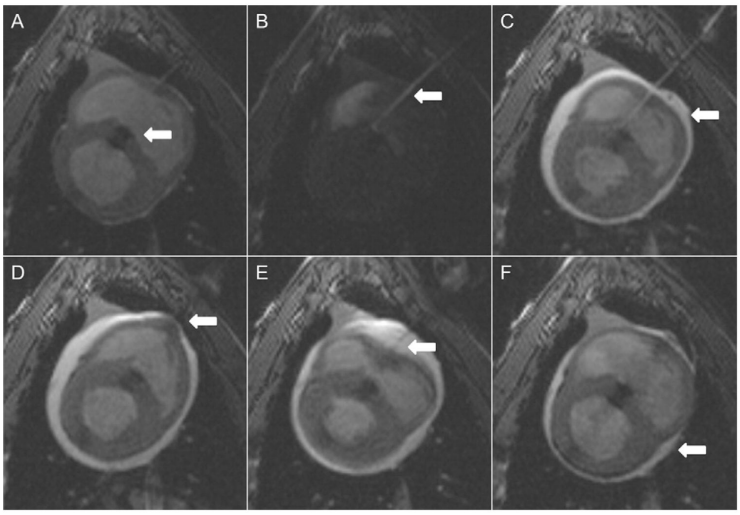


**Figure 4. Right Ventricular Free Wall Closure Performed With Vascular Closure Device Using Permissive Pericardial Tamponade Technique**

**(A)** Muscular ventricular septal defect closure device **(white arrow)** in good position. **(B)** Transthoracic access sheath **(white arrow)** position is confirmed with injection of dilute gadolinium. **(C)** Saline injected into pericardium **(white arrow)**. **(D)** Bioabsorbable co-polymer anchor is deployed through access sheath and pulled against right ventricular endomyocardial wall **(white arrow)**. **(E)** Collagen plug is deployed on epicardial surface and tamped in place **(white arrow)** through access sheath. **(F)** Evacuation of pericardial space **(white arrow)** (Online Video 4).

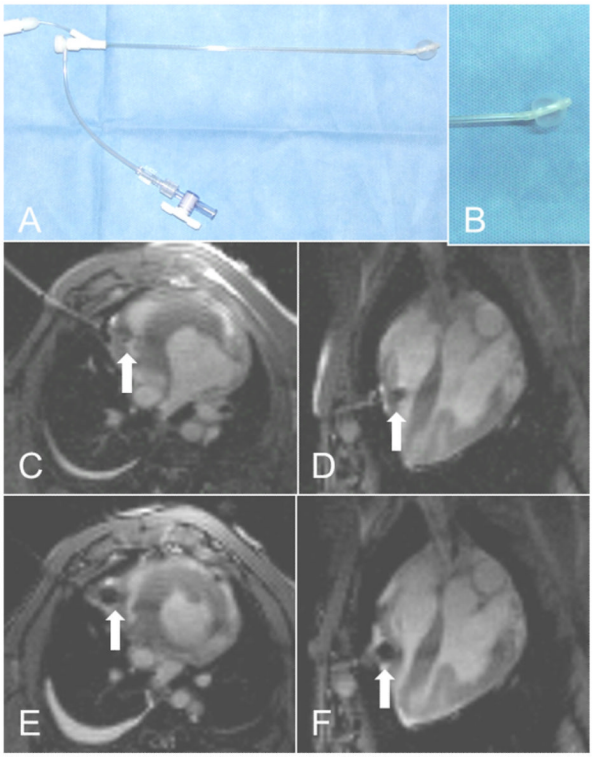


**Figure 5. Right Ventricular Access Sheath With Balloon Locking Mechanism**

**(A)** One potential "secure" transthoracic sheath (IABC, Cook Medical, Bloomington, Indiana). **(B)** Close-up shows the balloon inflated. **(C and D)** Short-axis and 4-chamber views showing transthoracic access sheath with balloon **(white arrow)** inflated in the right ventricle. **(E and F)** Short-axis and 4-chamber views showing transthoracic access sheath with balloon tip **(white arrow)** inflated for pericardial separation during right ventricular free wall closure.

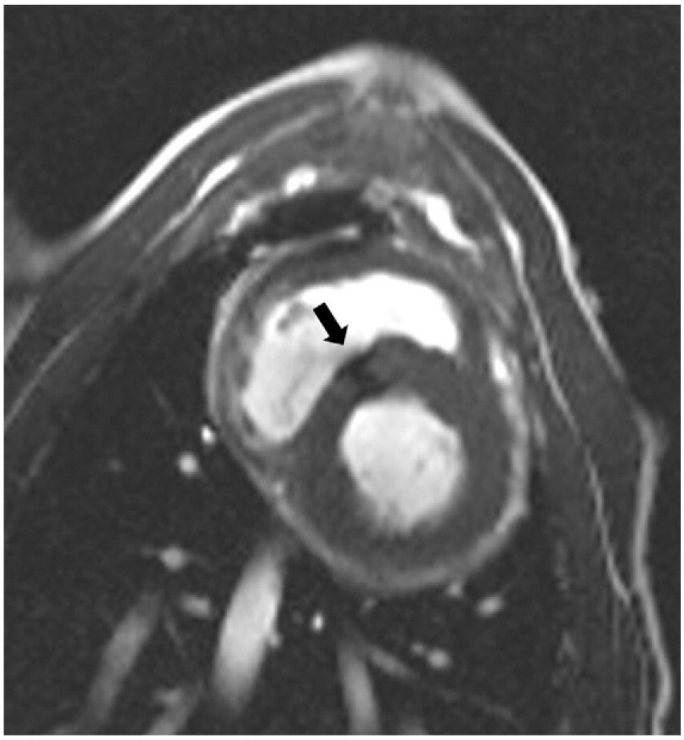

**Figure 6. MRI Demonstrating Successful Device Deployment and Right Ventricular Free Wall Closure at 1-Month Follow-Up**

SSFP "bright blood" image shows muscular VSD closure device **(black arrow)** in good position. Abbreviations as in Figure 1.

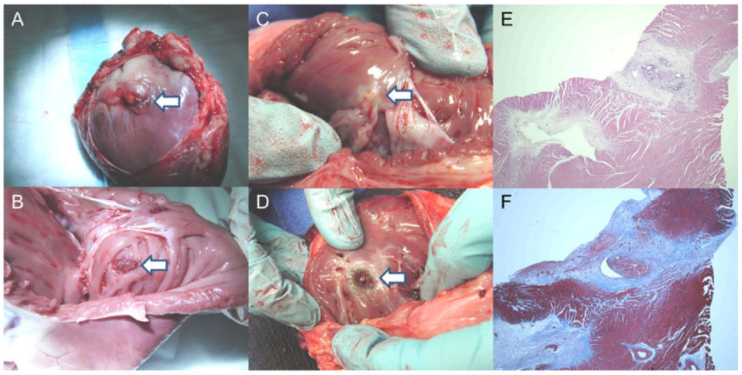


**Figure 7. Right Ventricular Free Wall: Gross Pathology and Histopathology**

**(A)** Vascular closure device (collagen plug is visible; **white arrow**) deployed on epicardial surface at 2 days. **(B)** Vascular closure device (copolymer anchor is visible; **white arrow**) deployed on endocardial surface at 2 days. **(C)** Vascular closure device **(white arrow)** on endocardial surface at 1 month. **(D)** ventricular septal defect occluder **(white arrow)** visible from right ventricle. **(E)** Hematoxylin and eosin stain of right ventricular free wall at percutaneous entry and closure site at 1 month shows foci of mature granulation tissue and foreign body giant cell reaction. **(F)** Trichrome stain (collagen colored **blue**) of right ventricular free wall at percutaneous entry and closure site at 1 month.

## Table 1

Procedural Details

| | Baseline (mm) (n = 8) | Post-muscular VSD Creation (n = 8) | Follow-Up | | | |
|---|---|---|---|---|---|---|
| | | | 1 h (n = 7) | 2 Days (n = 3) | 2 Weeks (n = 3) | 1 Month (n = 3) |
| Hemoglobin, g/dl | 7.5±0.7 | 7.2±0.5 | 8.1±1.9 | 8.1±0.5 | NA | 9.0±0.4 |
| Hematocrit, % | 22.0±2.1 | 21.1±1.6 | 23.8±5.4 | 23.7±1.5 | NA | 26.7±1.2 |
| Mean systemic blood pressure, mm Hg | 60.1±12.6 | 54.9±9.6 | 49.8±9.4 | 59.7±4.7 | NA | 68.0±2.6 |
| Pericardial effusion, mm | NA | 3.2±3.0 | 2.7±2.8 | 7.0±4.2 | 1.8±3.2 | 0.0±0.0 |
| Left pleural effusion, mm | NA | 0.3±0.9 | 1.0±1.8 | 0.0±0.0 | 0.0±0.0 | 0.9±1.5 |
| Right pleural effusion, mm | NA | 1.7±1.7 | 6.6±3.7 | 6.3±8.0 | 0.9±1.5 | 4.5±3.0 |
| Fick oximetry shunt quantification, Qp/Qs | 0.9±0.1 | 1.1±0.3 | 0.9±0.1 | 0.8±0.1 | NA | 1.0±0.1 |
| Phase-contrast shunt quantification, Qp/Qs | 1.0±0.0 | 1.2±0.2 | 0.9±0.0 | 1.0±0.0 | 1.0±0.0 | 1.0±0.0 |

Values are mean ± SD. NA = not applicable; Qp/Qs = pulmonary to systemic blood flow ratio; VSD = ventricular septal defect.